EXPERIMENTING WITH AUTONOMOUS CALIBRATION OF A CAMERA RIG ON A VISION SENSOR NETWORK

Kyung min Han, Yuanqiang Dong and Guilherme DeSouza
Department of Electrical and Computer Engineering, University of Missouri
349 Engineering Building West, Columbia, U.S.A.

Keywords: Vision sensor network, Image clustering, Global coordinate reference.

Abstract: This paper presents a completely autonomous camera calibration framework for a vision sensor network consisting of a large number of arbitrarily arranged cameras. In the proposed framework, a sequence of images for calibration is collected without a tedious human intervention. Next, the system automatically extracts all necessary features from the images and finds the best set of images that minimizes the error in 3D reconstruction considering all cameras in the set.

1 INTRODUCTION

Calibration of multiple camera systems became an important topic along with vision sensor networks (VSN) such as for: virtual and augmented reality; surveillance; battle field reconnaissance; etc. (Remagnino and Jones, 2002; Jaynes, 1999; Koller et al., 1997). In order to calibrate a VSN several critical steps must be taken: 1) acquiring images synchronously; 2) extracting feature points from the images; 3) establishing the correspondence among the feature points in multiple images from multiple cameras; 4) performing individual camera calibrations; and 5) computing a global coordinate reference for all cameras. Currently, a few of these steps still require a number of tedious and manual subtasks such as: selecting good images from which feature points can be extracted for calibration; manually establishing the correspondences between feature points from different cameras; etc. These tasks become quite challenging and time consuming especially when the VSN has a large number of cameras. Moreover, a great human involvement in the calibration process can induce errors that could lead to a poor overall accuracy of the system. Therefore, it is quite desirable that vision sensor networks can be autonomously calibrated.

In (Huang and Boufama, 2002), for example, a semi-automatic calibration system was developed for augmented reality. However, the method presented still requires that the user clicks on four points per image in order to construct homography matrices. Besides the tedious requirement of clicking on a large number of points, the user is also required to be very careful when performing this task. Otherwise, the accuracy of the calibration will degenerate with every point wrongly selected.

Another common approach is to resort to some special marker, such as a laser pointer (Svoboda et al., 2005) or a LED stick (Baker and Aloimonos, 2000). One of the main drawbacks of these kinds of systems is in the quite large number of images that must be obtained in order to cover a reasonable small space – since only one or two feature points can be obtained from each image.

In (Olsen and Hoover, 2001), a system to calibrate cameras in a hallway was proposed using several square tiles. Similar to the landmarks in (Koller et al., 1997), their method not only requires that several tiles be carefully positioned, but also that the area covered by the tiles spans the field of view of all cameras in the hallway.

A pattern-free approach was proposed in (Chen et al., 2005), where the trajectory of a bouncing ball is used for calibration. Yet their method is tested only using computer simulation and it is unclear whether their algorithm can perform at all in a real situation. Another pattern-free approach is the system described in (Yamazoe et al., 2006). In that case, a geometry constraint is used to extract feature points from a human silhouette. However, their method requires a traditional pre-calibration step in order to estimate the fundamental matrices used for the final calibration.

In this paper, we present a completely autonomous framework that performs optimal multi-camera cali-

min Han K., Dong Y. and DeSouza G. (2010).
EXPERIMENTING WITH AUTONOMOUS CALIBRATION OF A CAMERA RIG ON A VISION SENSOR NETWORK.
In *Proceedings of the 7th International Conference on Informatics in Control, Automation and Robotics*, pages 234-237
DOI: 10.5220/0002924802340237

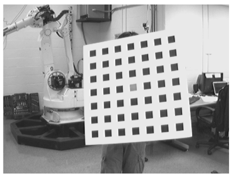

(a) original image

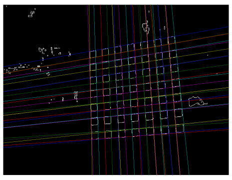

(b) detected lines

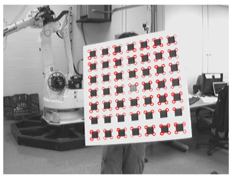

(c) detected features

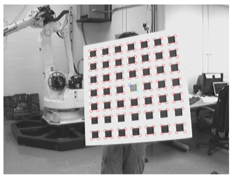

(d) final detected corners

Figure 1: Steps of the detection algorithm in (Han and DeSouza, 2007).

bration in terms of the final error in 3D reconstruction for any given subset of the cameras. In order to achieve that, the system only requires that a sequence of images be captured by the cameras while a human presents a calibration pattern at arbitrary poses in front of the cameras. Then the proposed algorithm automatically: searches for feature points on the pattern that will be used for calibration; selects the best set of images that optimizes the overall accuracy from calibration; and computes the individual camera calibrations as well as the best sequence of transformations from the camera to a global coordinate frame.

2 THE PROPOSED ALGORITHM

As we mentioned earlier, the proposed framework for the calibration of multiple cameras in a vision sensor network consists of several steps. In this paper we will focus only on steps 2, 3 and 5 above.

Figures 1(a)-(d) show the various steps of our **feature detection** algorithm developed in (Han and DeSouza, 2007). As illustrated by these figures, a small number of spurious lines and consequently spurious feature points are initially detected due to noise in the image. However, after a few more steps into the detection algorithm, all spurious feature points are eliminated, as depicted in Figure 1(d). Finally, given the shape of the pattern, the algorithm automatically establishes an order to each corner point. This ordering system is later used for **feature correspondence**.

The existence of noise in the images greatly affects the performance of the feature detection algorithm. Hence, it is necessary to evaluate these images, assign a score to them, and choose only those that can lead to the best calibration. The algorithm initially assigns a uniform score of 100 to every image acquired. Then, algorithm starts to deduct a penalty whenever the image fails to satisfy a certain expectation. To **rank the image**, the penalty is formulated as:

$$
\begin{aligned}
Score_j &= 100 - 100 \times \textstyle\sum_{i=1}^{n} p_i + s_i \times \mid N - n \mid \\
s_i &= max\left(stdv_{u_i}\right) + max\left(stdv_{v_i}\right) \\
p_i &= \frac{\left(stdv_{u_i} + stdv_{v_i}\right)}{N}
\end{aligned}
\qquad (1)
$$

Where $stdv_{u_i}$ and $stdv_{v_i}$ are the standard deviations in, respectively, the u and v coordinates of detected corners; N is the total number of corners in the pattern and n is the number of corners detected. The rationale behind this scoring scheme is to assign a penalty that is proportional to the uncertainty ($stdv$) in the detected feature point.

Once an image rank is created using the above scores, the algorithm must start selecting images for calibration. We **cluster the images** according to two non-exclusive criteria: orientation (*straight-centered, tilted-forward, tilted-backward, tilted-to-the-left and tilted-to-the-right*) of the pattern and its distance (*near, medium and far*) to the camera. The clustering of the images is performed by a K-means algorithm using the the angles of the edges and the pattern's apparent size. Once the clusters are formed, the algorithm selects for each camera calibration five images according to the rank $Score_j$. That is, one image from each of the five orientations is selected from the *medium* clusters. Next, two more images from the *near* and *far* clusters are selected based solely on their ranks – that is, these images can come from any of the five orientation clusters. Finally, two extra images of the pattern are selected for every pair of cameras that share a view of the pattern at that pose. Once the images are chosen, the calibration is performed using a popular method found in the literature (Zhang, 2000).

The final step of the algorithm is the problem of **finding the best transformation** from the coordinate frame of any camera i to any camera j. However, not all possible paths between cameras assure the same accuracy in 3D reconstruction. Due to the quality of the image used for calibration, some paths may lead to better accuracy than others. We approached this problem using a graph search algorithm which is the same as the problem of finding all-pairs shortest paths. We first compute the shortest-path where weights are scored as described above. Next we apply the Floyd-Warshall Algorithm (Floyd, 1962) to find the best path and therefore the best transformation between camera coordinate systems.

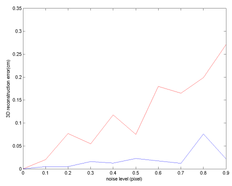

(a) no radial distortion

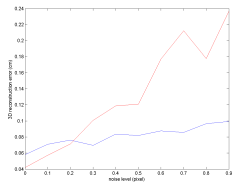

(b) with radial distortion

Figure 2: Errors of 3d reconstruction vs. levels of noise. Blue lines denote the errors using the best images and red lines denote the errors using poorly ranked images.

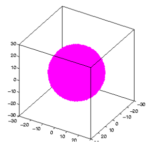

(a) synthetic sphere

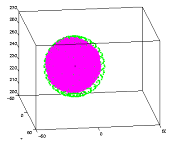

(b) real sphere

(c) human upper body in (Lam et al., 2009)

Figure 3: 3D Reconstructions.

3 EXPERIMENTAL RESULTS

We tested our proposed algorithm for two different situations. The first group of tests was done with synthetic data and we used from 6 to 42 virtual cameras. The second group of tests was done with real data using 6 cameras.

Using the intrinsic parameters from real cameras, we initially created a virtual space with 18 cameras – all pointing to the center of the space. We set the origin of this space at the center, so that the positions of all 18 cameras could be easily determined. These arbitrary intrinsic and extrinsic parameters of the cameras will later be referred to as our ground truth. Next, two thousand positions of the **synthetic** pattern were randomly generated and noise plus camera radial distortion were added at various levels to simulate the effects of real data. One last position of the pattern was created separately from the training set for testing purpose. The above procedure was repeated 10 times and the results were averaged over all trials.

The amount of noise and distortion added varied through the entire experiment. However, even when the amount of noise – the standard deviation of a white (Gaussian) noise – is 2 pixels, the algorithm still performs very well, with less than 1cm of error in 3D reconstruction. Also, in order to contrast the algorithm with a bad scenario in which the images for calibration are not appropriately selected, we compared the performance of the calibration using images that scored poorly. Figures 2(a) and (b) show the error in 3D reconstruction as a function of the noise. The error is calculated as the difference between the estimated (reconstructed) coordinates of the test points and the ground truth. Figure 2(a) shows the simulation performed without adding radial distortion, while for 2(b), a typical radial distortion (from the real lenses) of 0.3 was added.

We also tested our algorithm with **real** data. Using the calibration parameters obtained using the proposed algorithm and the pixel coordinates of a set of predefined points in space as perceived by all 6 cameras, we reconstructed the spatial coordinates of these points and compared the calculated values with the real ones.

The calibration error was measured by averaging the results for 20 different snapshots while presenting the reference points to all cameras. The reference points were exactly $50cm$ apart. Each snapshot was taken by all 6 cameras, so a total of 120 images were used for this test. The accuracy of the final calibration was determined by calculating the distance between two reference points. The accuracy in 3D reconstruction was $50.6264cm$ – or less than 1.5% of the actual distance. Also, the small standard deviation ($0.2498cm$) shows that the calibration obtained with our algorithm gives a very consistent 3D reconstruction. It is important to mention that, for the current baseline of the cameras, a deviation of a single pixel in the location of the marks on the ruler already incurs on an error of almost 3mm in the reconstruction.

4 3D OBJECT MODELING

Since the main application for our camera rig is for 3D object modeling, we tested the accuracy of the calibration by reconstructing a sphere based on the idea of visual hull (Laurentini, 1994) and the human body using an algorithm for multi-view 3D modeling presented in (Lam et al., 2009). As before, the tests were conducted for both synthetic data and real data.

In the first case, synthetic data, we created multiples of 6 virtual cameras $(6, 12, 18, \ldots)$ arbitrarily positioned around the object. By utilizing intrinsic and distortion parameters, we synthesized the images of a sphere (ball) with $20cm$ of radius. Using the voxel carving approach (Dyer, 2001), we reconstructed the sphere and measured its radius. In simple terms, this approach consists of: 1) defining a set of voxels in the 3D space; 2) marking each voxel according to the occupancy of the object as projected onto each of the

Table 1: Estimated radii vs. the number of virtual cameras.

# of virtual cameras	6	12	18	24	30	36	42
estimated radius (cm)	21.53	21.35	21.00	20.43	20.25	20.15	20.15

$6n$ image planes; and 3) finding the intersection of the occupancy for all $6n$ cameras. Table 1 shows the relationship between the reconstructed radii versus the number of cameras used for reconstruction. As expected, the error decreases as the number of cameras increases. That is because, among other reasons, the occupancy defined by each camera view forms a cone in space and the intersection of any subset of camera views approximates the sphere by the surface of such cones. Every time a new camera is added to the subset, the approximation becomes closer to the actual shape of the sphere. Since this procedure also relies on a sphere-fitting algorithm to circumscribe the occupied voxels, the detected radius tends always to be larger than the actual radius. For the real data, six cameras were used to take images of a ball. For each image, a circular Hough transform was used to detect the boundary and the 2D radius of the ball. As before, we relied on a voxel carving approach to reconstruct the ball. Figures 3(a) and (b) depict the reconstructed sphere for both synthetic data and real data. For the real ball, also with $20cm$ of radius, a 3D sphere was fitted and the radius was estimated. The performance of the framework using real cameras was $24.3cm$. Finally, Figure 3(c) depicts the result from our multi-view algorithm for 3D modeling.

5 CONCLUSIONS

We have presented a novel method for autonomous camera calibration of a multi-camera rig. The experimental results showed that the algorithm is vital in order to obtain good 3D reconstruction. That is, the algorithm's selection of the best images for calibration leads to an improved calibration of as much as ten times of that obtained without using the algorithm. Finally, an application for the camera rig was presented where a sphere was placed in the middle of the rig and a 3D representation of the same sphere was constructed with an error in reconstruction (real camera) approaching the theoretical (synthetic cameras) error.

REFERENCES

Baker, A. and Aloimonos, Y. (2000). Complete calibration of a multi-camera network. In *Proceedings of IEEE International Workshop on Omnidirectional Vision*. IEEE Computer Society.

Chen, K., Hung, Y., and Chen, Y. (2005). Calibrating a camera network using parabolic trajectories of a bouncing ball. In *Proceedings of IEEE International Workshop on VS-PETS*. IEEE Computer Society.

Dyer, C. (2001). Volumetric scene reconstruction from multiple views. In *Foundations of Image Understanding*. Kluwer.

Floyd, R. (1962). Algorithm 97: Shortest path. *Commun. ACM*, 5(6):345.

Han, K. and DeSouza, G. N. (2007). A feature detection algorithm for autonomous camera calibration. In *Proceedings of Fourth International Conference on Informatics in Control, Automation and Robotics*.

Huang, Z. and Boufama, B. (2002). A semi-automatic camera calibration method for augmented reality. In *Proceedings of IEEE International Conference on System, Man and Cybernetics*. IEEE Computer Society.

Jaynes, C. (1999). Multi-view calibration from planar motion for video surveillance. In *Proceedings of IEEE International Workshop on Visual Surveillance*. IEEE Computer Society.

Koller, D., Klinker, G., Rose, E., Breen, D., Whitaker, R., and Tuceryan, M. (1997). Automated camera calibration and 3d egomotion estimation for augmented reality applications. In *Proceedings of the 7th International Conference on Computer Analysis of Images and Patterns*. Springer-Verlag.

Lam, D., Hong, R., and DeSouza, G. (2009). 3d human modeling using virtual multi-view stereopsis from on-the-fly motion estimation. In *Proceedings of IEEE/RSJ International Conference on Intelligent Robots and Systems*. IEEE Computer Society.

Laurentini, A. (1994). The visual hull concept for silhouette-based image understanding. *IEEE Transactions on Pattern Analysis and Machine Intelligence*.

Olsen, B. and Hoover, A. (2001). Calibrating a camera network using a domino grid. *Pattern Recognition*, 34.

Remagnino, P. and Jones, G. (2002). Registration of surveillance data for multi-camera. In *IEEE International Conference on Information Fusion*. IEEE Computer Society.

Svoboda, T., Martinec, D., and Pajdla, T. (2005). *A convenient multicamera self-calibration for virtual environments*. MIT Press, Cambridge.

Yamazoe, H., Utsumi, A., and Abe, S. (2006). Multiple camera calibration with bundled optimization using silhouette geometry constraints. In *Proceedings of the 18th International Conference on Pattern Recognition*. IEEE Computer Society.

Zhang, Z. (2000). A flexible new technique for camera calibration. *IEEE Transactions on Pattern Analysis and Machine Intelligence*.